OXFORD

Cerebral Cortex, April 2020;30: 2070–2082

doi: 10.1093/cercor/bhz223
Advance Access Publication Date: 10 January 2020
Original Article

ORIGINAL ARTICLE

Active Sleep Promotes Coherent Oscillatory Activity in the Cortico-Hippocampal System of Infant Rats

Carlos Del Rio-Bermudez[1], Jangjin Kim[1], Greta Sokoloff[1,2] and Mark S. Blumberg[1,2,3,*],

[1]Department of Psychological and Brain Sciences, University of Iowa, Iowa City, IA 52242, USA, [2]Iowa Neuroscience Institute, University of Iowa, Iowa City, IA 52242, USA and [3]Interdisciplinary Graduate Program in Neuroscience, University of Iowa, Iowa City, IA 52245, USA

Address correspondence to Mark S. Blumberg. Email: mark-blumberg@uiowa.edu

Abstract

Active sleep (AS) provides a unique developmental context for synchronizing neural activity within and between cortical and subcortical structures. In week-old rats, sensory feedback from myoclonic twitches, the phasic motor activity that characterizes AS, promotes coherent theta oscillations (4–8 Hz) in the hippocampus and red nucleus, a midbrain motor structure. Sensory feedback from twitches also triggers rhythmic activity in sensorimotor cortex in the form of spindle bursts, which are brief oscillatory events composed of rhythmic components in the theta, alpha/beta (8–20 Hz), and beta2 (20–30 Hz) bands. Here we ask whether one or more of these spindle-burst components are communicated from sensorimotor cortex to hippocampus. By recording simultaneously from whisker barrel cortex and dorsal hippocampus in 8-day-old rats, we show that AS, but not other behavioral states, promotes cortico-hippocampal coherence specifically in the beta2 band. By cutting the infraorbital nerve to prevent the conveyance of sensory feedback from whisker twitches, cortical-hippocampal beta2 coherence during AS was substantially reduced. These results demonstrate the necessity of sensory input, particularly during AS, for coordinating rhythmic activity between these two developing forebrain structures.

Key words: REM sleep, barrel cortex, myoclonic twitching, functional connectivity, development

Introduction

In the infant and adult nervous system, coupled neural oscillations support the efficient transfer of information across distant but functionally related networks (Buzsáki and Draughn 2004; Uhlhaas and Singer 2010; Brockmann et al. 2011; Fujisawa and Buzsáki 2011; Hartung et al. 2016a). In the developing sensorimotor system, neural oscillations are largely triggered by input from the sensory periphery (Khazipov et al. 2004; An et al. 2014; Tiriac et al. 2014; Akhmetshina et al. 2016; Del Rio-Bermudez et al. 2017). The sources of sensory input to the developing sensorimotor system include passive stimulation from external sources (i.e., exafference) and sensory feedback from self-generated movements (i.e., reafference; Khazipov et al. 2004; An et al. 2014; Tiriac et al. 2014; Del Rio-Bermudez et al. 2015; Akhmetshina et al. 2016; Tiriac and Blumberg 2016; Dooley and Blumberg 2018; Mukherjee et al. 2018).

Reafference can arise from wake movements or from myoclonic twitches, which occur abundantly and exclusively during active sleep (AS or REM sleep). Importantly, reafference from twitches triggers cascades of neural activity throughout the sensorimotor system at ages when wake-related movements largely fail to do so (Blumberg et al. 2013; Blumberg 2015; Tiriac and Blumberg 2016; Dooley and Blumberg 2018); this twitch-triggered activity includes neural oscillations (for review, see Del Rio-Bermudez and Blumberg 2018). Because oscillations assist in such neurodevelopmental processes as neuronal differentiation and migration, apoptosis, and somatotopic map formation (Khazipov and Luhmann 2006; Hanganu-Opatz 2010; Kilb et al. 2011; Blanquie et al. 2017a, 2017b), twitch-related

oscillatory activity is poised to contribute to the activity-dependent development of sensorimotor networks (Khazipov et al. 2004; Blumberg et al. 2013; Del Rio-Bermudez and Blumberg 2018).

Given the effects of twitch-related reafference on neural activity within individual sensorimotor structures, we hypothesized that twitches also promote oscillatory coupling across distant structures. Indeed, we previously demonstrated coherent, twitch-related theta-band (4–8 Hz) activity in the hippocampus and red nucleus (Del Rio-Bermudez et al. 2017). Here, we test the hypothesis that twitches play a causal role in such coupling, this time focusing on the network comprising the cortical whisker "barrel" field (S1-BF) and hippocampus. We focus on this network because 1) previous studies in rat pups have demonstrated that both barrel cortex (McVea et al. 2012; Tiriac et al. 2012; Akhmetshina et al. 2016) and hippocampus (Mohns and Blumberg 2008, 2010; Del Rio-Bermudez et al. 2017) exhibit twitch-related activity and 2) it is relatively easy to eliminate sensory feedback in the whisker system (Tiriac et al. 2012; Akhmetshina et al. 2016).

In the developing barrel cortex, sensory inputs drive two distinct patterns of oscillatory activity: spindle bursts (which exhibit a dominant frequency of ~15 Hz but comprise oscillations from 4 to 30 Hz) and early gamma oscillations (30–50 Hz; Akhmetshina et al. 2016; Luhmann and Khazipov 2018). In the developing hippocampus, twitches are associated with bursts of oscillatory activity at theta, beta, and gamma frequencies (Mohns and Blumberg 2008; Del Rio-Bermudez et al. 2017), and twitch-related activity in sensorimotor cortex is conveyed to the hippocampus via entorhinal cortex (Mohns and Blumberg 2010). All together, these findings suggest that twitches are well-suited to promote the flow of information through the cortico-hippocampal network.

Here, we show that unlike periods of active wake and behavioral quiescence (BQ), AS-related whisker twitches drive oscillatory coupling between barrel cortex and the CA1 area in hippocampus (Hipp CA1). Moreover, we find that twitches promote coupling specifically at beta2 frequencies (i.e., 20–30 Hz). To assess causality, we eliminated sensory feedback from the whiskers by transecting the infraorbital nerve (ION) and, by doing so, significantly and specifically reduced beta2 coherence during AS. Altogether, our findings demonstrate that AS-related sensory processing provides a critical context for the expression of functional connectivity within the developing cortico-hippocampal system.

Methods

Subjects

A total of 26 male and female Sprague-Dawley Norway rats (*Rattus norvegicus*) at postnatal day (P) 7–9 (hereafter P8) were used. Mothers and litters were housed in standard laboratory cages (48 × 20 × 26 cm). Animals were maintained on a 12:12 light-dark schedule with lights on at 07:00 h and with water and food available ad libitum. Litters were culled to eight pups at P3. Littermates were never assigned to the same experimental group. All experiments were conducted in accordance with the National Institutes of Health (NIH) Guide for the Care and Use of Laboratory Animals (NIH Publication No. 80-23) and were approved by the Institutional Animal Care and Use Committee of the University of Iowa.

Surgery

A pup with a visible milkband was prepared for neurophysiological recording using previously described methods (Blumberg et al. 2015). Briefly, under 2–5% isoflurane anesthesia, a stainless-steel head-fix apparatus was glued to the skull with cyanoacrylate adhesive gel. Bipolar electromyographic (EMG) electrodes (50 µm diameter; California Fine Wire, Grover Beach, CA) were implanted bilaterally into the nuchal muscle and in the maxillolabialis muscle contralateral to the neural recording sites. The surgical procedure lasted 15–20 min. After surgery, the pup was transferred to an incubator and maintained at thermoneutrality (35 °C) for 1 h to recover. The pup was briefly anesthetized again to drill holes in the skull under stereotaxic guidance (David Kopf Instruments, Tujunga, CA) to allow for later insertion of electrodes into S1-BF (coordinates in relation to bregma, anteroposterior (AP): −1.5 mm; mediolateral (ML) ±4.5 mm; dorsoventral (DV) −0.5 to −0.9 mm; 15° lateral angle) and Hipp CA1 (coordinates in relation to bregma, AP: −2 mm; ML: ±1.5 mm; DV: −2 to −2.5 mm; 15° latero-frontal angle). Two additional holes were drilled: one in frontal cortex for insertion of a thermocouple and the other in lateral visual cortex, contralateral to the recording sites, for insertion of a chlorinated silver ground wire (which was also used as the reference electrode).

General Procedure and Neurophysiological Recordings

The pup was transferred to a testing chamber where its head was fixed within a stereotaxic apparatus and its torso was secured to a narrow platform with limbs dangling freely on each side. A fine-wire thermocouple (Omega Engineering, Stamford, CT) was inserted into the frontal cortex to monitor brain temperature, which was maintained at 36–37 °C throughout the recording session. Neural data were acquired using 16-channel silicon depth electrodes (NeuroNexus, Ann Arbor, MI; A4 × 4–3 mm-100-177) connected to a data acquisition system (Tucker-Davis Technologies, Alachua, FL). Neural and EMG signals were sampled at 25 and 1 kHz, respectively. Before insertion, electrodes were coated with fluorescent DiI (Vybrant DiI Cell-Labeling Solution; Life Technologies, Grand Island, NY) for subsequent histological verification of placement.

Spontaneous and Evoked Activity in S1-BF and Hippocampus

A total of 14 pups were tested for spontaneous and evoked activity in S1-BF and Hipp CA1. Each pup was acclimated in the stereotaxic apparatus for at least 90 min, by which time it was cycling between sleep and wake. Before recording began and to assess electrode placement, we confirmed that stimulation of the whiskers yielded consistent S1-BF neural responses. Stimuli consisted of brief air puffs delivered to the vibrissae contralateral to the neural recording sites. Air puffs were delivered through a flat-end needle attached to a plastic tube placed approximately 1 cm away from the whisker pad. Stimulus duration (50 ms) and pressure (10–15 psi) were controlled using a solenoid valve connected to a pulse stimulator (A-M Systems, Sequim, WA). Using this procedure, air puffs reliably resulted in a forward deflection of the whiskers. After sensory responses were confirmed, spontaneous activity in S1-BF and Hipp CA1 was recorded for at least 30 min, which at this age is sufficient to capture dozens of sleep-wake transitions and hundreds of twitches (Blumberg et al. 2004, 2005). During this time, the experimenter (blind to the electrophysiological recording on the com-

puter screen) scored the pup's wake movements and twitches using computer key presses. At the end of the session, neural responses to sensory stimulation of the whiskers were systematically assessed: Air puffs were delivered for 10 min (interstimulus interval = 5 s, yielding ~120 air puffs per recording session) and the onset of each stimulus was registered on the computer.

Transection of the Infraorbital Nerve

Twelve additional pups ($n = 6$ per group) were used to assess the effects of ION transection on the role of twitches in the functional connectivity between S1-BF and Hipp CA1. Each pup was prepared for testing as described above. In addition, the ION was exposed and visualized using a small retraction hook. Transections of the ION were performed using small scissors at the level of the infraorbital foramen. Sham operations involved exposure and manipulation of the nerve without cutting it. After a postsurgery recovery period of at least 1 h, the pup was transferred to a stereotaxic apparatus, and neural activity in both S1-BF and Hipp CA1 was recorded over a period of 30 min as described above.

Histology

After testing, the pup was overdosed with ketamine/xylazine (0.08 mg/g IP) and perfused transcardially with phosphate-buffered saline and 4% paraformaldehyde. The brain was sliced coronally at 80 µm using a freezing microtome (Leica Microsystems, Buffalo Grove, IL). Electrode locations were visualized at ×2.5–5 magnification using a fluorescent microscope and digital camera (Leica Microsystems). Following fluorescent photography, cortical sections were stained for cytochrome oxidase (CO), which has been shown in rats as young as P5 to reliably delineate primary sensory areas (Seelke et al. 2012). Briefly, cytochrome c (3 mg per 10 mL solution), catalase (2 mg per 10 mL solution; Sigma-Aldrich), and 3,3′-diaminobenzidine tetrahydrochloride (5 mg per 10 mL solution; Spectrum) were dissolved in a 1:1 solution of phosphate-buffered distilled water. Sections were developed in well plates on a shaker table at 35–40 °C for 3–6 h. Sections were then washed and mounted.

Quantification and Statistical Analysis

All analyses and statistical tests of neural data were performed using custom-written MATLAB routines (MathWorks, Natick, MA), Spike2 software (Cambridge Electronic Design), and SPSS (IBM, Armonk, NY). Data were tested for normality using the Kolmogorov–Smirnov test. When data were not normally distributed, nonparametric tests were used. Alpha was set at 0.05 for all analyses, unless otherwise stated; when appropriate, the Bonferroni correction procedure was used. Group data are presented as mean ± standard error (SE).

Behavioral State

Using EMG signals and manually scored behavior, the assessment of behavioral state was conducted using methods previously described (Blumberg et al. 2015; Del Rio-Bermudez et al. 2016). AS was defined by the presence of myoclonic twitches against a background of muscle atonia. Active wake (AW) was defined by the presence of high-amplitude limb movements against a background of high muscle tone. Finally, BQ was defined as the period between the end of active wake and the beginning of active sleep when muscle tone is low (for at least 1 s), there is an absence of spiking activity in the EMG, and there are no twitches. This period can also be referred to as quiet sleep; however, because cortical slow waves are not evident until P11 (Seelke and Blumberg 2008), it is not possible at P8 to definitively distinguish between quiet wake and quiet sleep. Accordingly, the state is designated here as BQ.

Spike Sorting

The neurophysiological record was band-pass filtered (500–5000 Hz). Spike sorting was performed using template matching and principal component analyses in Spike2. Waveforms differing from the template by more than 3.5 standard deviations were considered outliers and were excluded from further analysis (Sokoloff et al. 2015). Because it was necessary to lower the electrodes using a fronto-lateral angle, the electrode shanks in S1-BF were not perpendicular to the cortical surface. This made it difficult to determine the layer-specific location of each electrode site. Thus, we pooled the units for analysis.

State-Dependent Firing Rates

For each recorded neuron in S1-BF and Hipp CA1, we determined mean firing rates across AS, AW, and BQ. On rare occasions (<10%), units exhibiting firing rates exceeding 2.5 times the standard deviation within a behavioral state were treated as outliers and were excluded from analysis. Average firing rates for each behavioral state within either structure were averaged across units in all pups. Wilcoxon matched-pairs signed-ranks test were used to compare firing rates across behavioral states in both structures.

State-Dependent LFP Power Spectrum

For all local field potential (LFP)-related analyses, one channel per pup from each structure was randomly selected. LFP signals were down-sampled to 500 kHz, and a DC-remove filter (time constant: 0.1 s) was applied. Power spectra were calculated using a 500-ms Hanning window (bin size: 1.9 Hz) in Spike2. For time-normalization and subsequent statistical comparisons, the spectral power density values in each bin were divided by the total duration of the file comprising data for each behavioral state. LFP power within each structure was normalized to the maximal power within the 4–50-Hz frequency range across behavioral states. State-dependent differences in LFP power were calculated using repeated-measures ANOVA with power in each frequency range—theta, alpha/beta, beta2, and slow gamma (sgamma: 30–50 Hz)—as the repeated measure.

Twitch-Related and Sensory-Evoked Neural Activity

The temporal relationship between whisker twitches and unit activity in the S1-BF and Hipp CA1 was examined. First, for each unit, we generated perievent histograms (10-ms bins, 1-s windows) using whisker twitches as trigger events. Statistical significance was calculated by jittering twitch events 1000 times within a 500-ms window using PatternJitter (Harrison and Geman 2009; Amarasingham et al. 2012) implemented in MATLAB. Briefly, PatternJitter is a resampling method that analyzes the statistical structure of spike trains by randomizing patterns of successive events while preserving their overall "firing" structure and short-range statistics. Next, we generated upper and lower acceptance bands for each event correlation ($P < 0.05$ for each band; Amarasingham et al. 2012). Only units that exceeded the significance threshold were used to construct twitch correlations in each structure. Data were normalized within each

individual correlation, smoothed using a 10-ms time constant, and averaged across pups.

To examine twitch-related responses in the LFP, we first looked at LFP power immediately following twitches (500-ms post-twitch window). Individual twitch-triggered time-frequency spectrograms were generated using a complex Morlet wavelet. To create the Morlet wavelet, the frequency band of interest (4–50 Hz) was divided into 30 bins, and the temporal resolution of the wavelet was determined using 2–3 cycles. Twitch-triggered LFP waveforms within the beta2 range were calculated as follows: First, raw neural signals were filtered using a 20–30 Hz finite impulse response (FIR) band-pass filter. Next, the signal was converted using root mean square (time constant: 0.1 s). Using whisker twitches as trigger events, waveform averages of beta2 activity for both structures within the same pup were calculated using a peri-twitch window of 1 s. To assess the temporal relation between twitch-triggered beta2 oscillations in S1-BF and Hipp CA1, we calculated the latency between twitch onset and peak response in the beta2 oscillation for each structure. Average latencies for each structure were averaged across pups. To calculate statistical differences between peak latencies, we used paired *t* tests.

Multiunit activity and LFP responses to sensory stimulation of the whiskers were calculated using the methods described above. LFP data from three pups were excluded from analysis due to noise in the signal during whisker stimulation.

Coherence and PLI

For coherence analyses, data across the three behavioral states (AS, AW, and BQ) were segmented into 2-s bins, and coherence values were calculated for each bin and averaged within each state using custom-written MATLAB scripts. Coherence was calculated from cross-spectral density using the following formula:

$$C(f) = \frac{\sum_{i-1}^{N} X_i(f)\, Y_i^*(f)}{\sqrt{\sum_i^N |X_i(f)|^2 \sum_i^N |Y_i(f)|^2}}$$

where $C(f)$ represents the complex-valued coherence, $X_i(f)$ and $Y_i(f)$ are the Fourier transforms of the signals X and Y for the data segment i at frequency f, and * indicates the complex conjugate.

Each signal was convolved using a complex Morlet wavelet. The Morlet wavelet was created as follows: The frequency band of interest (4–50 Hz) was divided into 50 bins and the temporal resolution of the wavelet was determined using 4–8 cycles. To calculate state-dependent differences in coherence, we performed repeated-measure ANOVA with average coherence within each frequency band across behavioral states. Twitch-triggered coherence values (500-ms post-twitch window) from real data were compared with twitch-triggered coherence calculated with shuffled data. For this, we used a bootstrap-shuffle method applied to the Hipp CA1 LFP; in each iteration ($n = 1000$), we selected a random point on the LFP and switched the 2-s segments on either side of that point (Del Rio-Bermudez et al. 2017). To determine the contribution of twitches to the observed coherence in the beta2 band, we calculated the ratio of theta and beta2 coherence during AS and 500 ms after twitches. Theta/beta2 ratios of original and shuffled data were compared using independent-samples *t* tests.

To assess the possibility that oscillatory coupling was not due to volume conduction from a common source, we calculated the phase lag index (PLI) between AS-related beta2 oscillations in S1-BF and Hipp CA1. PLI measures the asymmetry of the distribution of phase differences between two oscillatory signals at a given frequency and detects the partial contribution of volume conduction to coherence measures (Stam et al. 2007). First, we filtered the LFP signals in both structures using an FIR filter (20–30 Hz). PLI was then calculated using the following formula:

$$PLI = \left|\langle \text{sign}\ [\Delta\phi(t_k)]\rangle\right|$$

where $\Delta\phi(t_k)$ represents the phase differences of a time series. This index ranges between 0 and 1, where 0 indicates that there is no lag between the phase of two oscillations at a particular frequency (thus possibly reflecting volume conduction from a common source) and 1 indicates a constant phase difference between the two oscillations. PLI values for each pup were statistically tested against the null hypothesis ($PLI = 0$) using one-sample *t* tests. It should be noted that zero-phase lag synchronization for oscillations in distant brain areas does not necessarily rule out functional connectivity between two structures (Vicente et al. 2008; Gollo et al. 2014).

Effects of Transection of the Infraorbital Nerve

We assessed whether ION transection affected sleep times and twitching rates. Total time spent in AS and twitch rates (number of whisker twitches per unit time in AS) were calculated for each pup and averaged across pups in the same experimental group (Nerve Cut and Sham). Next, we calculated firing rates for each unit in S1-BF and Hipp CA1 across behavioral states and averaged them for each experimental group. Twitch-related unit activity was analyzed as described above, and the percentage of significant twitch-related units in each structure was compared across experimental groups using chi-squared tests. Changes in LFP power after ION transection were calculated as follows: First, normalized power within each frequency of interest was extracted from the power spectrum for each behavioral state. Next, the percent increase in LFP power during AS was compared with BQ. Statistical differences between experimental groups were compared using independent-sample *t* tests for each frequency band. Finally, coherence values between LFP signals in S1-BF and Hipp CA1 across behavioral states and following twitches for each frequency band were calculated as described above and compared between groups using independent-samples *t* tests. Based on our initial finding that oscillatory coherence between S1-BF and Hipp CA1 was specifically promoted at beta2 frequency and to minimize variations in the signal across groups, we selected for further analysis the LFP channel in S1-BF with maximal beta2 frequency power and the first LFP channel in Hipp CA1 that was dorsal to the location of the reversal potential (i.e., stratum pyramidale).

For all within-subject effects in repeated-measures analyses, Greenhouse–Geisser corrections were applied when the assumption of sphericity of the data was violated.

Results

Neural Activity Increases During AS in the Neonatal Cortico-Hippocampal System

We recorded extracellular activity simultaneously in S1-BF and Hipp CA1 in P8 rats ($n = 14$). Histology confirmed electrode

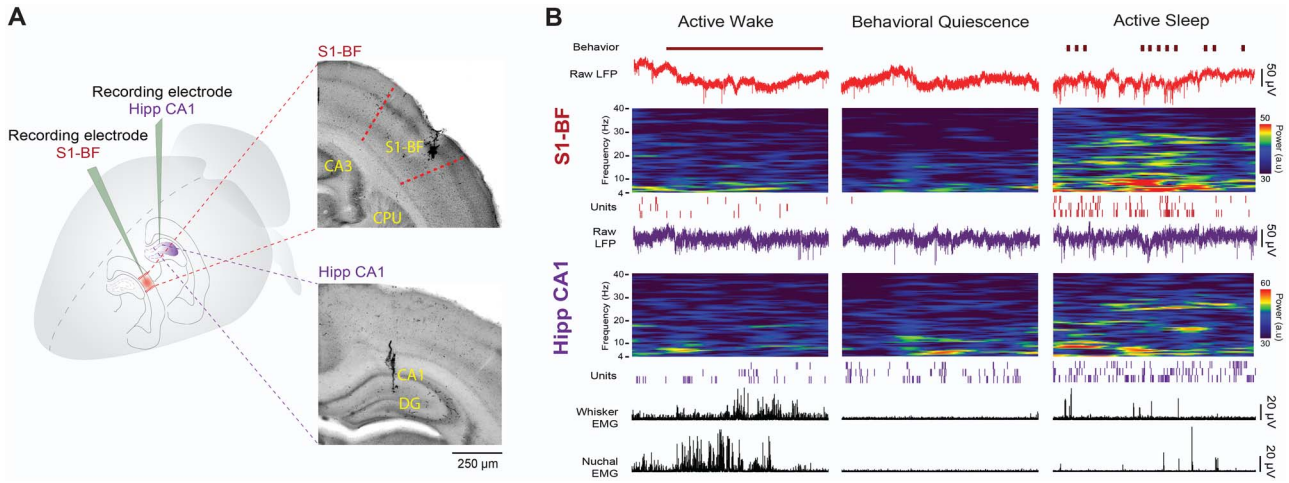

Figure 1. Neural activity in the cortico-hippocampal system across behavioral states at P8. (*A*) Illustration depicting simultaneous electrode placements in the S1 barrel field (S1-BF) and CA1 region of hippocampus and, at right, corresponding CO-stained coronal sections for a representative pup. DG: dentate gyrus; CPU: caudate-putamen. (*B*) Representative data in a P8 rat showing manually scored sleep and wake behavior (wake movements: horizontal red line; twitches: red ticks), raw LFP, time-frequency spectrograms, and unit activity (S1-BF, red traces; Hipp CA1, purple traces), and whisker and forelimb EMGs.

placements in both structures (Fig. 1A). Activity in both structures was most prominent during AS, including the presence of spindle bursts in S1-BF (Fig. 1B). Spindle bursts were heterogeneous, with oscillatory components in the theta, alpha/beta, beta2, and sgamma bands (Fig. S1A–C), consistent with previous reports in visual and somatosensory cortices (Hanganu et al. 2007; Yang et al. 2016). In addition, as previously described (Alhbeck et al. 2018), oscillatory bursts in Hipp CA1 were similarly heterogeneous, with the dominant frequency in the theta band along with irregular, lower-amplitude components in the beta and sgamma bands (Fig. S1D–F).

Firing rates in S1-BF were significantly higher in AS than in AW and BQ ($n = 117$ units; $P_s < 0.001$; Fig. 2A, top). Similarly, firing rates in Hipp CA1 ($n = 90$ units) were significantly higher in AS than in AW and BQ ($P_s < 0.001$; Fig. 2A, bottom). LFP power was also highest during AS in both structures (Fig. 2B). Specifically, in S1-BF, power in the theta ($F_{(1.2,15.5)} = 13.2$, $P < 0.005$), beta2 ($F_{(2,26)} = 40.6$, $P < 0.001$), and sgamma ($F_{(2,26)} = 24.6$, $P < 0.001$) bands was significantly higher in AS than in AW or BQ ($P_s < 0.05$; Fig. 2C, top); alpha/beta power was significantly higher only in relation to BQ ($F_{(2,26)} = 9.2$, $P < 0.005$; pairwise comparison $P < 0.001$). In Hipp CA1, power in the alpha/beta ($F_{(1.4,18.7)} = 19.2$, $P < 0.001$), beta2 ($F_{(1.2,16.2)} = 38.8$, $P < 0.001$), and sgamma ($F_{(1.2,15.4)} = 43.06$, $P < 0.001$) bands was significantly higher in AS than in AW or BQ ($P_s < 0.005$, Fig. 2C, bottom).

We next asked whether AS-related neural activity in this network is specifically related to whisker twitches. As shown in Figure 3, twitches were associated with increases in single-unit and LFP activity in both S1-BF and Hipp CA1. Figure 3A shows representative (left) and averaged (right) twitch-related responses in the two structures. In S1-BF and Hipp CA1, 27.3% (32/117) and 11.1% (10/90) of recorded units, respectively, exhibited significant increases in firing rates in response to whisker twitches ($P_s < 0.05$), with twitch-related unit activity exhibiting shorter latencies in S1-BF (76 ± 10 ms) than in Hipp CA1 (178 ± 30 ms; $t_{(41)} = -3.6$, $P < 0.005$). Spectrograms in Figure 3B illustrate the brevity of LFP bursts in both structures across frequency bands in response to whisker twitches.

Whisker Twitches During AS Promote Coherent Oscillations in the Cortico-Hippocampal Whisker System

Having shown thus far that beta2 activity increases significantly in both S1-BF and Hipp CA1 during AS, we next determined whether beta2 coherence across the two structures also increases during AS. Indeed, beta2 coherence was significantly greater in AS than in AW or BQ ($F_{(2,26)} = 16.2$, $P < 0.001$); this was also true for the sgamma band ($F_{(2,26)} = 8.0$, $P < 0.005$; Fig. 4A,B). The only other significant effect involved increased alpha/beta coherence in BQ in relation to AW ($F_{(2,26)} = 5.8$, $P < 0.01$). Moreover, PLI values for beta2 coupling during AS were significantly different from zero (0.097 ± 0.001; $t_{(13)} = 47.9$, $P < 0.001$), suggesting that the observed coherence was not due to volume conduction from a common source (Stam et al. 2007).

We next determined whether increased beta2 coherence during AS was specifically related to whisker twitches. Although coherence in the post-twitch period was reduced overall in comparison with AS (Fig. 4C), post-twitch coherence was selectively enhanced in the beta2 band. This selectivity is evident from the beta2/theta coherence ratio, which was significantly greater during post-twitch periods as compared with AS ($F_{(1,13)} = 7.0$, $P < 0.05$) or shuffled data ($F_{(1,13)} = 5.1$, $P < 0.05$; Fig. 4D).

The mean twitch-triggered beta2 waveform in S1-BF exhibited a narrower, shorter-latency peak than that in Hipp CA1 (Fig. 4E); moreover, peak latencies were shorter in S1-BF than in Hipp CA1 (mean latency: 71.1 ± 10.9 vs. 106.9 ± 10.1 ms; $t_{(26)} = -2.3$, $P < 0.05$; Fig. 4F). Along with the unit-related latencies described above, these observations are consistent with previous findings in infant (Mohns and Blumberg 2010) and adult (Pereira et al. 2007) rats showing that sensory feedback from whiskers is conveyed from sensory cortex to hippocampus.

Because exafferent stimulation is also a potent driver of neural activity in the neonatal sensorimotor system (Tiriac et al. 2014; Del Rio-Bermudez et al. 2015; Akhmetshina et al. 2016), we also determined whether manual stimulation of the whiskers elicits similar coherence patterns to those observed after whisker twitches (Fig. S2A). In response to contralateral whisker stimulation, we observed brief increases

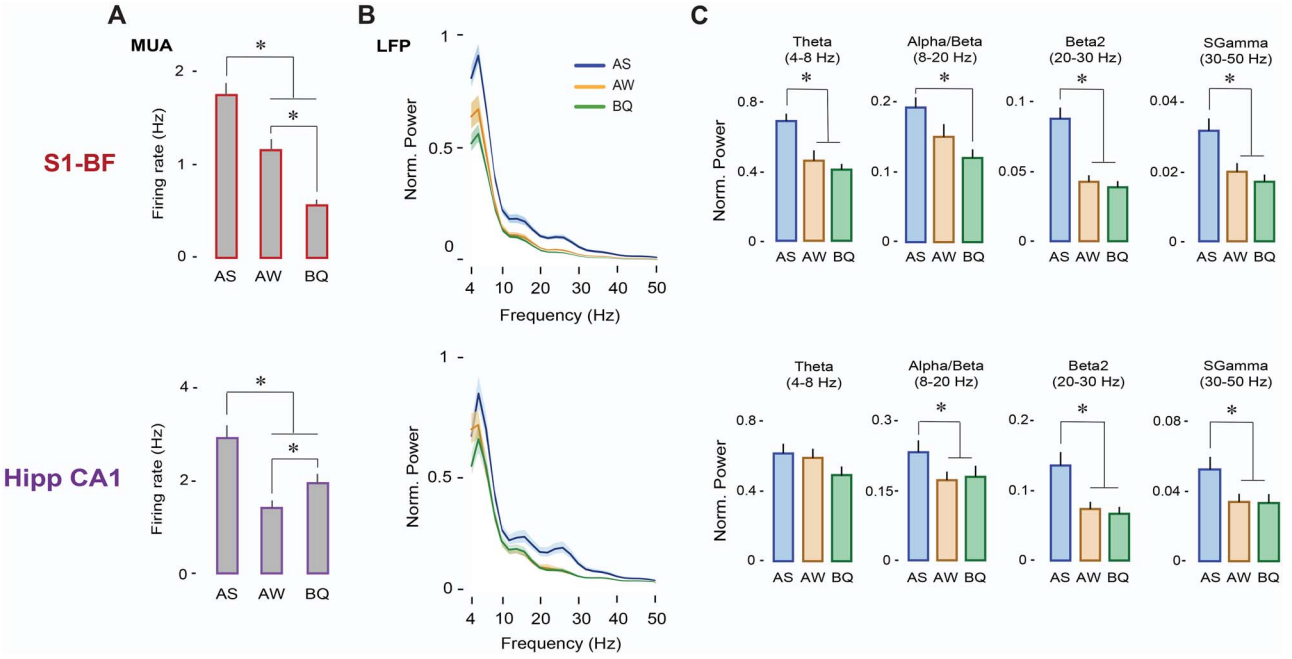

Figure 2. Neural activity in S1-BF and Hipp CA1 is expressed maximally during AS. (*A*) Mean (+SE) firing rates during AS, AW, and BQ for neurons in S1-BF ($n = 117$ units, top) and Hipp-CA1 ($n = 90$ units, bottom). * denotes significant difference from other states ($P < 0.001$). (*B*) Mean (±SE) LFP power spectra for S1-BF (top) and Hipp CA1 (bottom) during AS (blue), AW (orange), and BQ (green). (*C*) Mean LFP power (+SE) in S1-BF ($n = 14$ LFPs, top) and Hipp CA1 ($n = 14$ LFPs, bottom) across frequency bands and behavioral states (AS, AW, BQ). * denotes significant difference from AW and/or BQ ($P < 0.005$).

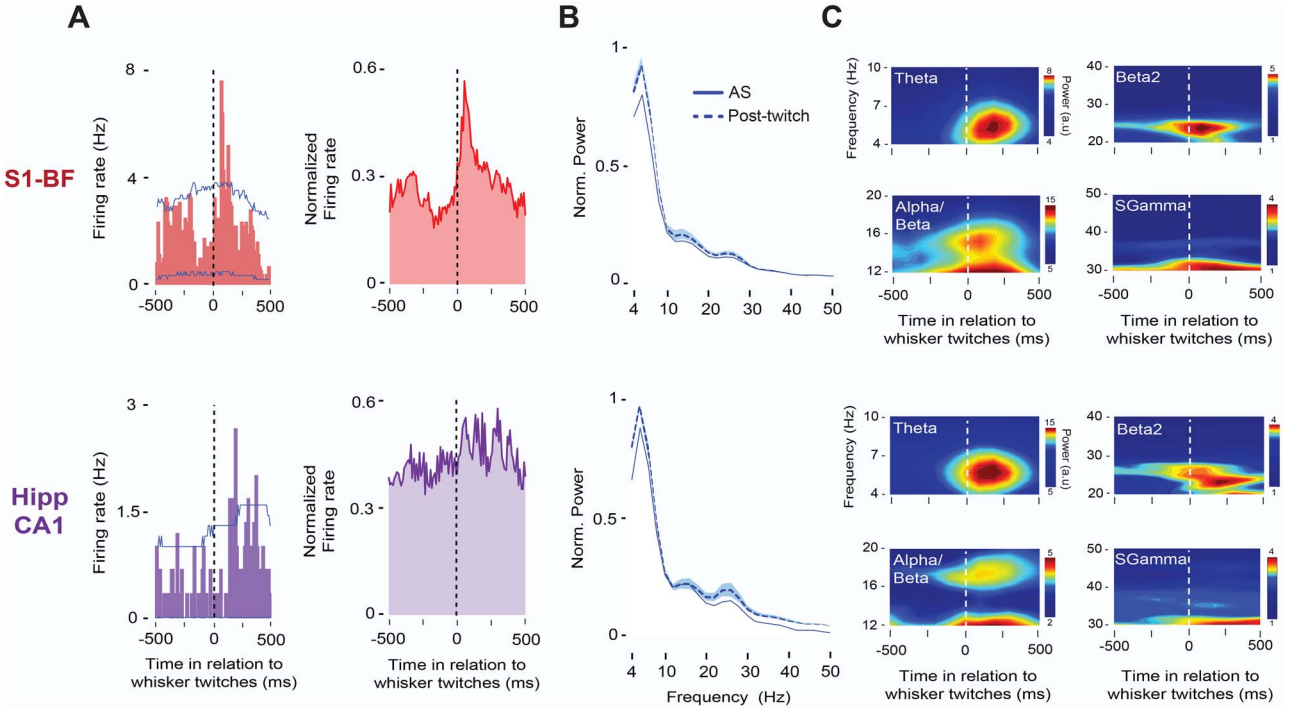

Figure 3. Whisker twitches during AS drive neural activity in S1-BF and Hipp CA1. (*A*) Left: Representative perievent histograms (10-ms bins) for spike activity in relation to whisker twitches in S1-BF (red, top) and Hipp CA1 (purple, bottom) in a P8 rat. Vertical dashed lines indicate twitch onset. Upper and lower acceptance bands ($P < 0.05$ for each band) are indicated by blue lines. Right: Same as at left but for normalized pooled data across those units in S1-BF ($n = 32$) and Hipp CA1 ($n = 10$) that exhibited significant twitch-related activity ($P < 0.05$). (*B*) Mean LFP power spectra (+SE) for AS (solid line) and post-twitch periods (500-ms window, dashed line) for S1-BF ($n = 14$, top) and Hipp CA1 ($n = 14$, bottom) from the same P8 rat. (*C*) Representative twitch-triggered time-frequency spectrograms for S1-BF (top) and Hipp CA1 (bottom) from the same P8 rat. Vertical dashed lines in spectrograms denote whisker twitch onset.

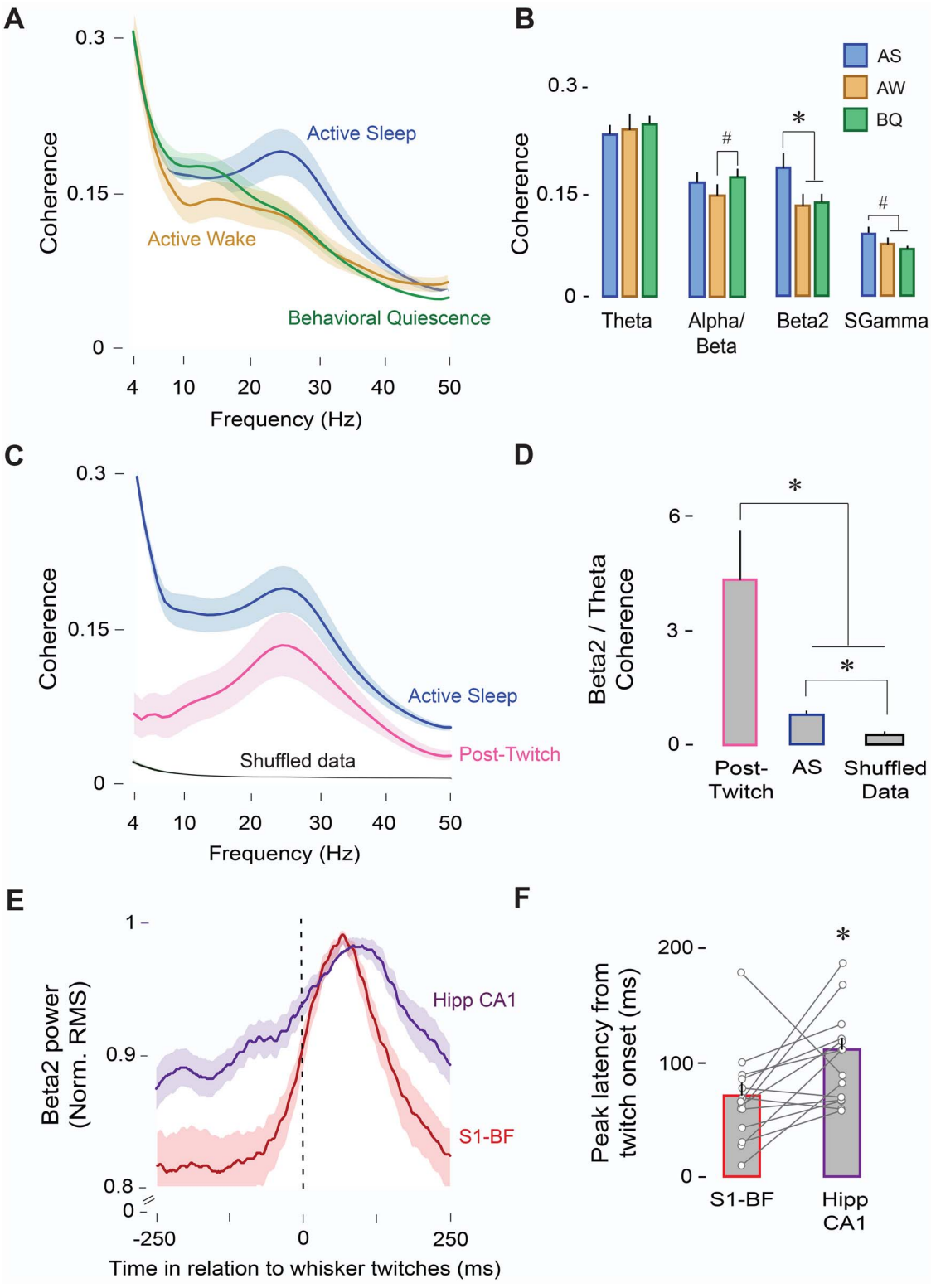

Figure 4. AS enables oscillatory coupling between S1-BF and Hipp CA1. (*A*) Mean LFP-LFP coherence spectra between S1-BF and Hipp CA1 ($n = 14$ pups, 14 LFP pairs) during AS (blue), AW (orange), and BQ (green). Shaded area indicates SE. (*B*) Mean (+ SE) LFP-LFP coherence values across frequency bands and behavioral states (AS, AW, and BQ). * denotes significant difference ($P < 0.01$). # denotes significant difference ($P < 0.05$). (*C*) Mean LFP-LFP coherence spectra between S1-BF and Hipp CA1 ($n = 14$ pups, 14 LFP pairs) during AS (blue), post-twitch periods (500-ms window, pink), and shuffled data (black). Shaded area indicates SE. (*D*) Mean beta2/theta ratios for coherence values during AS, post-twitch periods, and shuffled data. * denotes significant difference ($P < 0.05$). (*E*) Mean normalized twitch-triggered LFP power (beta2; 20–30 Hz; root mean square) pooled across subjects (14 pups, 14 LFPs) for S1-BF (red) and Hipp CA1 (purple). Shaded area indicates SE. Vertical line denotes whisker twitch onset. (*f*) Mean (+ SE) peak latency in (*E*) for S1-BF (red) and Hipp CA1 (purple). Vertical lines depict latency data from individual pups. * denotes significant difference ($P < 0.05$).

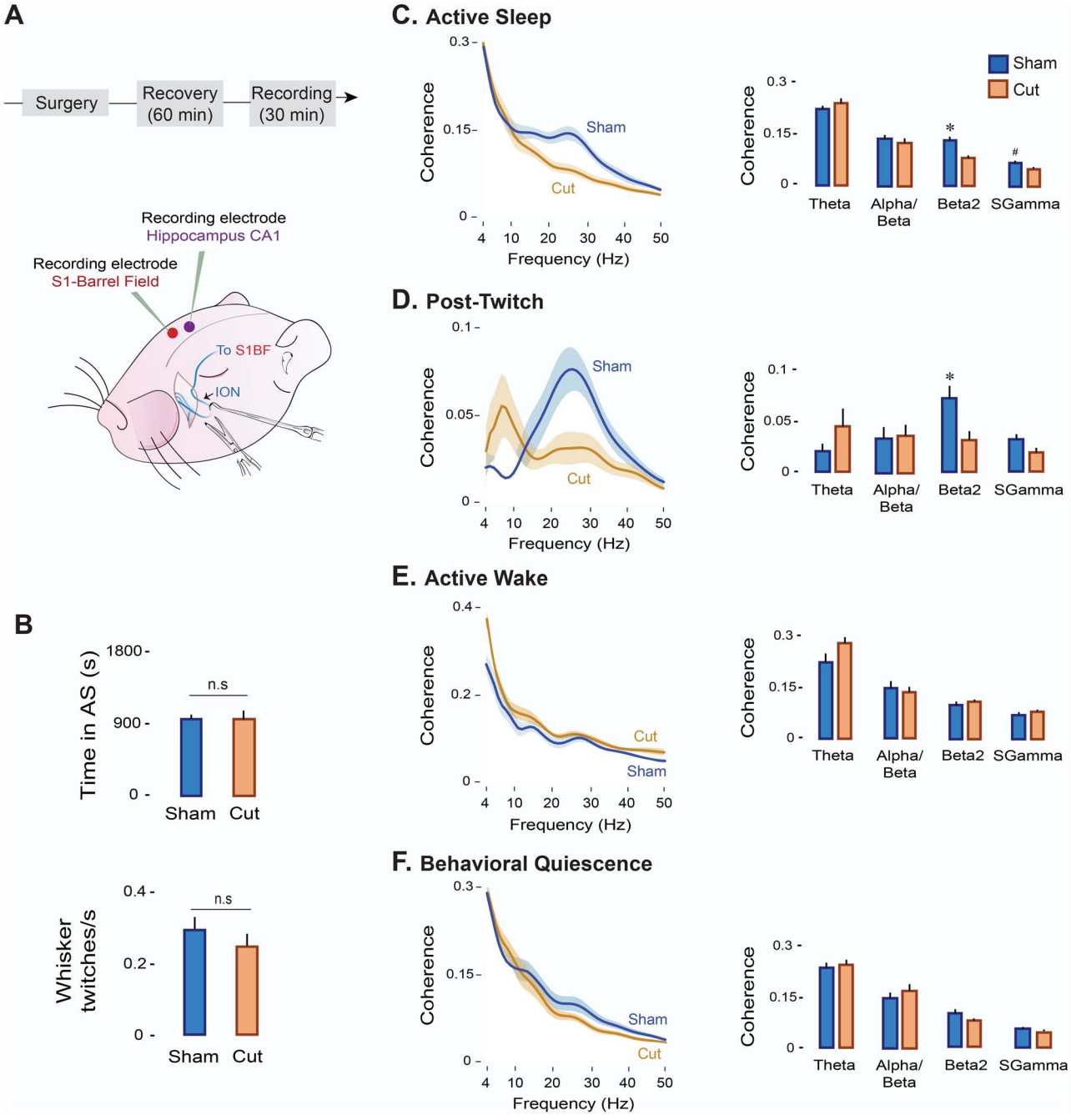

Figure 5. Transection of the ION decreases oscillatory coupling between S1-BF and Hipp CA1 in a state-dependent manner. (*A*) Experimental timeline and illustration depicting ION transections in a P8 rat. (*B*) Mean (+SE) time spent in AS (top) and whisker twitching rates (bottom) in the Sham ($n = 6$ pups, blue) and Cut ($n = 6$ pups, orange) experimental groups. n.s: not significant. (*C*) Left: Mean LFP-LFP coherence spectra between S1-BF and Hipp CA1 during AS in the Sham ($n = 6$ pups, 6 LFP pairs; blue line) and Cut ($n = 6$ pups, 6 LFP pairs; orange line) groups. Shaded area indicates SE. Right: Mean (+ SE) LFP-LFP coherence values across frequency bands in the Sham (blue) and Cut (orange) groups. (*D*) Same as in (*C*) but for post-twitch activity during AS (post-twitch window: 500 ms). (*E*) Same as in (*C*) but for AW. (*f*) Same as in (*C*) but for BQ.

in single-unit and LFP activity in both S1-BF and Hipp CA1 (Fig. S2*B*). Specifically, 71.7% of S2-BF units (84/117) and 14.4% of hippocampal units (13/90) exhibited significant increases in firing rate after whisker stimulation ($P_s < 0.05$; Fig. S2*C*). Power spectra in S1-BF and Hipp CA1 immediately after stimulation were similar to the spectra observed for AS and twitching, with peaks in the theta, alpha/beta, and beta2 frequency bands (Fig. S2*D*). Finally, coherence analyses revealed a significant peak at beta2 frequency in relation to shuffled data ($t_{(20)} = 4$, $P < 0.005$; Fig. S2*E*). Although we observed marked increases in beta2 activity in response to whisker stimulation in both structures (Fig. S2*F*), their latencies in relation to stimulus onset were not significantly different. Overall, these data support the notion that both exafferent and reafferent signals effectively activate developing sensorimotor circuits (Akhmetshina et al. 2016).

Coherent Beta2 Oscillations in the Cortico-Hippocampal Whisker System Rely on Sensory Feedback From Twitches

To assess the causal role of twitching in promoting beta2 coherence in S1-BF and Hipp CA1, we transected or sham-transected the contralateral ION in P8 rats ($n = 6$ per group; Fig. 5A). ION transections did not affect the mean amount of time spent in AS or whisker twitching rates in relation to shams (Fig. 5B). In contrast, ION transections produced significant state-dependent reductions in S1-BF firing rates ($P_s < 0.001$; Fig. S3A) and in the percentage of twitch-related units ($\chi^2(1, N = 107) = 19.8$, $P < 0.0001$; Fig. S3B). Also, although LFP power spectra for the two structures were similar in the two experimental groups across behavioral states (Fig. S3C,E), ION transections produced a selective reduction in cortical beta2 power during AS ($t_{(10)} = -2.3$, $P < 0.05$; Fig. S3D); no power reductions were observed in Hipp CA1 (Fig. S3F).

Along with the reduction in cortical beta2 power during AS, transection of the ION had a profound effect on cortico-hippocampal coherence. Specifically, in the transected pups, coherence during AS was significantly reduced in both the beta2 ($t_{(10)} = -3.9$, $P < 0.005$) and sgamma ($t_{(10)} = -2.4$, $P < 0.05$) bands (Fig. 5C). In addition, as shown in Figure 5D, twitch-related coherence after ION transection was markedly reduced only in the beta2 band ($t_{(10)} = -2.8$, $P < 0.2$). In contrast, ION transection did not significantly affect coherence during AW or BQ in any frequency band ($P_s > 0.05$; Fig. 5E,F).

Discussion

We have proposed that AS provides a unique developmental context for synchronizing neural activity within and between cortical and subcortical structures (Del Rio-Bermudez and Blumberg 2018). Previously, recording from hippocampus and red nucleus, we showed that the two structures are maximally coherent during AS in the theta band (Del Rio-Bermudez et al. 2017). Here, recording from hippocampus and barrel cortex, we show that these two structures are maximally coherent during AS in the beta2 band. In addition, by transecting the nerve that conveys sensory feedback from the whiskers to barrel cortex, we specifically eliminated beta2 coherence between the two structures. Our results indicate that AS—and particularly AS-related twitching—promotes oscillatory coupling in the cortico-hippocampal system.

We propose that this early coupling lays a foundation for the contributions of this system to such later-emerging adult capacities as spatial navigation and context representation (Pereira et al. 2007; Igarashi et al. 2014).

Sleep-Dependent Neural Activity in the Developing Cortico-Hippocampal System

Early oscillatory activity is thought to play a fundamental role in the development of the nervous system (Khazipov et al. 2004; Khazipov and Luhmann 2006; Hanganu-Opatz 2010; Brockmann et al. 2011; McVea et al. 2012; Benders et al. 2015; Wikstrom et al. 2015; Yang et al. 2016; Hartung et al. 2016b; Del Rio-Bermudez et al. 2017; Lebedeva et al. 2017; Valeeva et al. 2018; Del Rio-Bermudez and Blumberg 2018). Based on studies using in vitro preparations or anesthetized rat pups in vivo, one might conclude that the functional value of coherent activity is independent of behavioral state. In contrast, we have advocated for the critical importance of sleep-wake states for properly assessing neural activity and functional connectivity at these early ages (Del Rio-Bermudez et al. 2017; Del Rio-Bermudez and Blumberg 2018). Moreover, when behavioral state is taken into account, it is clear that oscillations in developing cortical and subcortical sensorimotor networks preferentially occur during AS (Lahtinen et al. 2002; Mohns and Blumberg 2008, 2010; Tiriac et al. 2014; Del Rio-Bermudez et al. 2017). Here, in agreement with previous studies in the somatosensory cortex (Tiriac et al. 2014; Tiriac and Blumberg 2016) and hippocampus (Lahtinen et al. 2002; Mohns and Blumberg 2008; Del Rio-Bermudez et al. 2017) of neonatal rats, we found that firing rates and LFP power in barrel cortex and hippocampus are highest during AS. In addition, oscillatory coupling between the two structures is substantially greater during AS.

AS-related increases in cortical and hippocampal activity could be explained by several factors. For example, neurotransmitter dynamics vary across behavioral states, giving rise to different levels and patterns of neural activity. In the cortico-hippocampal system, AS is associated with the increased release of acetylcholine (Marrosu et al. 1995; Teles-Grilo Ruivo et al. 2017). Cholinergic inputs contribute to various neurodevelopmental processes in cortical and hippocampal networks, including synaptic plasticity and apoptosis (Lipton and Kater 1989; Pugh and Margiotta 2000; Maggi et al. 2003). They also modulate oscillatory activity in developing networks. For example, in the visual cortex during the first postnatal week, blockade of muscarinic receptors in vivo decreases spindle burst activity (Hanganu et al. 2007). Conversely, in vitro administration of carbachol (a cholinergic receptor agonist) in the neonatal S1-BF induces transient oscillations at 10–30 Hz (Kilb and Luhmann 2003).

Due to a gating mechanism within the caudal medulla that persists through P11 (Dooley and Blumberg 2018), sensory feedback from wake-related movements is not conveyed to such downstream structures as sensorimotor cortex (Tiriac et al. 2014; Tiriac and Blumberg 2016; Dooley and Blumberg 2018) and hippocampus (Del Rio-Bermudez et al. 2017). This gating mechanism appears to preclude oscillatory coupling during wake, as shown here and in a previous study (Del Rio-Bermudez et al. 2017).

Disruption of Sensory Feedback Blocks AS-Dependent Oscillatory Coupling Between Barrel Cortex and Hippocampus

Blocking whisker-related reafference with transections of the ION exerted differential effects in barrel cortex and hippocampus. In barrel cortex, nerve transections caused a marked decrease of firing rates during AS and AW, states characterized by the presence of whisker movements. During AS, we also observed a selective reduction of cortical oscillations in the beta2 band, emphasizing the role of sensory feedback in the generation of these oscillations. On the other hand, nerve transections did not markedly affect hippocampal activity, perhaps because the neonatal hippocampus receives projections from a wide array of inputs (Mohns and Blumberg 2008, 2010; Del Rio-Bermudez et al. 2017; Valeeva et al. 2018). Thus, disrupting sensory input within a single modality seems not to be sufficient to affect overall hippocampal activity. Regardless, in the absence of sensory input from the whiskers, the oscillatory coupling between barrel cortex and hippocampus that normally occurs during AS was blocked.

Disruption of peripheral sensory input decreases oscillatory events and firing rates in the developing spinal cord (Inácio et al. 2016), sensory thalamus (Tiriac et al. 2012), and cortex (Khazipov and Luhmann 2006; Yang et al. 2016). These studies typically report an approximately 50% reduction in neural activity after peripheral sensory blockade, leading to the conclusion that sensory input is not necessary for the remaining 50% of activity. However, the effect of sensory blockade on higher-order aspects of neural activity was not previously examined. Our results demonstrate that blockade of sensory feedback not only reduces local neural activity in a state-dependent manner, but also impairs the coupling of neural activity across a developing sensorimotor network.

Anatomical Pathways Supporting Synchronization of Sensory-Dependent Neural Activity in Barrel Cortex and Hippocampus

In processing sensory information from the external environment, the adult hippocampus constructs and updates spatial representations of the environment (Moser et al. 2017) and modulates sensory-guided motor behavior and navigation (Bland and Oddie 2001). In rats and other rodents, such sensory information is largely provided by the whisker system.

Whisker-related sensory signals reach hippocampal CA1 via cortical inputs from barrel cortex (Pereira et al. 2007; Mohns and Blumberg 2010; Itskov et al. 2011). Consistent with our results, Pereira et al. (2007) showed that electrical stimulation of the ION and mechanical stimulation of the whiskers in adult rats trigger responses in hippocampal CA1 neurons with significantly longer latencies and wider response curves than those in barrel cortex; pharmacological inactivation of barrel cortex decreased these sensory-evoked responses in hippocampal CA1. Similarly, in the hippocampus of week-old rats, reafferent and exafferent responses follow cortical responses and depend upon an intact anatomical connection with sensory cortex (Mohns and Blumberg 2010).

Peripheral sensory inputs to hippocampal CA1 from sensory cortex are conveyed through the perirhinal and entorhinal cortices (Vinogradova 2001; Pereira et al. 2007; Mohns and Blumberg 2010; Bellistri et al. 2013; Valeeva et al. 2018). If twitch-related responses in hippocampal CA1 are transferred from barrel cortex through these pathways, one might expect twitches to drive similar neural responses in sites along the S1-to-CA1 pathway. Indeed, a recent study in rat pups demonstrated that sensory feedback from self-generated movements synchronizes network activity in the medial entorhinal cortex and hippocampus (Valeeva et al. 2018). Movement-evoked bursts of unit activity in the medial entorhinal cortex that preceded hippocampal activity were accompanied by increased LFP power in the beta-gamma frequency range. These LFP responses in the medial entorhinal cortex are consistent with our finding that sensory inputs drive beta2 oscillations in barrel cortex that are then conveyed to the hippocampus via entorhinal cortex.

Interestingly, the activity-dependent anatomical and functional development of the hippocampal-entorhinal system follows a linear sequence that mimics this natural flow of information from the cortex to the hippocampus—starting in layer II of medial entorhinal cortex and sequentially propagating along the CA3-CA1-dentate gyrus-subiculum pathway and then back to deeper layers of entorhinal cortex (Donato et al. 2017). Collectively, the present results suggest that sensory feedback from twitches during AS provide the necessary excitatory inputs to activate the S1-to-CA1 pathway, thus orchestrating the emergence of coordinated activity and promoting activity-dependent plasticity in this network.

Beta2 Oscillations in the Infant and Adult Cortico-Hippocampal Network

The present results indicate that early cortico-hippocampal oscillatory coherence during AS and in response to sensory stimulation is most notably expressed in the beta2 band. Beta2 oscillations have been previously described in vivo in the sensory cortex and hippocampus of adult (Baker 2007; Martin et al. 2007; Berke et al. 2008; França et al. 2014; Igarashi et al. 2014; Rangel et al. 2015; Vinck et al. 2016) and neonatal (Lahtinen et al. 2002; Luhmann and Khazipov 2018; Valeeva et al. 2018) rodents.

Cortical beta2 oscillations can be elicited by olfactory (Martin et al. 2007) and whisker stimulation (Hamada et al. 1999). From a functional perspective, cortical beta oscillations engage motor and sensory networks and are thought to support cortico-muscular coherence and sensorimotor integration (Baker 2007). Hippocampal beta2 oscillations can also be elicited by external stimuli, such as task-relevant reward cues (Rangel et al. 2015). In the mouse hippocampus, 20–30 Hz oscillations in hippocampal CA1 have been observed during exploration of novel contexts and objects, and are likely involved in the initial encoding and representation of new environments and unexpected sensory stimuli (Berke et al. 2008; Grossberg 2009; França et al. 2014).

In adult rats, maximal oscillatory coherence between the entorhinal cortex and hippocampal CA1 occurs at 20–40 Hz. This activity correlates positively with behavioral performance in a spatial associative memory task (Igarashi et al. 2014). In addition, oscillatory coupling between barrel cortex and hippocampal CA1 during locomotion also peaks at these frequencies, suggesting that beta oscillations synchronize activity between cortical and hippocampal networks during movement (Vinck et al. 2016).

Finally, the present findings are consistent with a previous report showing a 20–30 Hz rhythm during AS in the neonatal rat hippocampus (Lahtinen et al. 2002). They also provide the first evidence that AS-dependent beta2 oscillations promote oscillatory coupling between sensory cortex and hippocampus in early development.

Conclusions

Early oscillatory activity plays important roles in the development of the nervous system. In the sensorimotor cortex of neonatal rats, the amount of oscillatory activity affects the rate of apoptosis, a key contributor to the development and refinement of neural networks (Lebedeva et al. 2017; Blanquie et al. 2017b). In premature human infants, the prevalence of cortical oscillations is related to subsequent brain growth and cognitive development (Benders et al. 2015; Wikstrom et al. 2015). In addition, coordinated or synchronous patterns of early electrical activity between distant but functionally related neural structures is a hallmark of emerging network connectivity (Uhlhaas et al. 2010; Brockmann et al. 2011; Hartung et al. 2016b; Del Rio-Bermudez et al. 2017; Del Rio-Bermudez and Blumberg 2018; Valeeva et al. 2018; Gretenkord et al. 2019).

Here we have demonstrated that the expression and synchronization of early oscillatory activity in the sensorimotor system relies heavily on AS-related sensory input. Consequently, any condition that disrupts sleep or sensory processing could be detrimental to the typical development of local circuits and

long-range connectivity. In the whisker system of rat pups, for instance, early sensory deprivation leads to anatomical and functional alterations of the barrel cortex and results in behavioral impairments that can persist into adulthood (Simons and Land 1987; Fox 1992; Crocker-Buque et al. 2015). In addition, in adult rodents, sleep deprivation alters synaptic plasticity in sensorimotor cortex, hippocampus, and cerebellum (Sei et al. 2000; Abel et al. 2013; Li et al. 2017). Thus, to the extent that sleep and sleep-related sensory processing contribute to the typical development of the sensorimotor system, disrupted sleep may cause or exacerbate the sensorimotor deficits that characterize a variety of neurodevelopmental disorders, including autism (Nebel et al. 2012; Whyatt and Craig 2013).

Funding

This research was supported by the National Institute of Child Health and Human Development grant R37-HD081168 to M.S.B. C.D.R.-B was supported by the Fulbright Foreign Student Program.

Notes

Conflict of Interest: None declared.

References

Abel T, Havekes R, Saletin JM, Walker MP. 2013. Sleep, plasticity and memory from molecules to whole-brain networks. *Curr Biol*. 23:R774–R788.

Akhmetshina D, Nasretdinov A, Zakharov A, Valeeva G, Khazipov R. 2016. The nature of the sensory input to the neonatal rat barrel cortex. *J Neurosci*. 36:9922–9932.

Alhbeck J, Song L, Chini M, Bitzenhofer SH, Hanganu-Opatz IL. 2018. Glutamatergic drive along the septo-temporal axis of hippocampus boosts prelimbic oscillations in the neontal mouse. *elife*. 7:e33158.

Amarasingham A, Harrison MT, Hatsopoulos NG, Geman S. 2012. Conditional modeling and the jitter method of spike resampling. *J Neurophysiol*. 107:517–531.

An S, Kilb W, Luhmann HJ. 2014. Sensory-evoked and spontaneous gamma and spindle bursts in neonatal rat motor cortex. *J Neurosci*. 34:10870–10883.

Baker SN. 2007. Oscillatory interactions between sensorimotor cortex and the periphery. *Curr Opin Neurobiol*. 17:649–655.

Bellistri E, Aguilar J, Brotons-Mas JR, Foffani G, De la Prida LM. 2013. Basic properties of somatosensory-evoked responses in the dorsal hippocampus of the rat. *J Physiol*. 591:2667–2686.

Benders MJ, Palmu K, Menache C, Borradori-Tolsa C, Lazeyras F, Sizonenko S, Dubois J, Vanhatalo S, Hüppi PS. 2015. Early brain activity relates to subsequent brain growth in premature infants. *Cereb Cortex*. 25:3014–3024.

Berke JD, Hetrick V, Breck J, Greene RW. 2008. Transient 23–30 Hz oscillations in mouse hippocampus during exploration of novel environments. *Hippocampus*. 18:519–529.

Bland BH, Oddie SD. 2001. Theta band oscillation and synchrony in the hippocampal formation and associated structures: the case for its role in sensorimotor integration. *Behav Brain Res*. 127:119–136.

Blanquie O, Kilb W, Sinning A, Luhmann HJ. 2017a. Homeostatic interplay between electrical activity and neuronal apoptosis in the developing neocortex. *Neuroscience*. 358:190–200.

Blanquie O, Yang J-W, Kilb W, Sharopov S, Sinning A, Luhmann HJ. 2017b. Electrical activity controls area-specific expression of neuronal apoptosis in the mouse developing cerebral cortex. *elife*. 6:e27696.

Blumberg MS. 2015. Developing sensorimotor systems in our sleep. *Curr Dir Psychol Sci*. 24:32–37.

Blumberg MS, Marques HG, Iida F. 2013. Twitching in sensorimotor development from sleeping rats to robots. *Curr Biol*. 23:R532–R537.

Blumberg MS, Middlemis-Brown JE, Johnson ED. 2004. Sleep homeostasis in infant rats. *Behav Neurosci*. 118:1253–1261.

Blumberg MS, Seelke AMH, Lowen SB, Karlsson KA. 2005. Dynamics of sleep-wake cyclicity in developing rats. *Proc Natl Acad Sci*. 102:14860–14864.

Blumberg MS, Sokoloff G, Tiriac A, Del Rio-Bermudez C. 2015. A valuable and promising method for recording brain activity in behaving newborn rodents. *Dev Psychobiol*. 57:506–517.

Brockmann MD, Pöschel B, Cichon N, Hanganu-Opatz IL. 2011. Coupled oscillations mediate directed interactions between prefrontal cortex and hippocampus of the neonatal rat. *Neuron*. 71:332–347.

Buzsáki G, Draughn A. 2004. Neuronal oscillations in cortical networks. *Science*. 304:1926–1929.

Crocker-Buque A, Brown SM, Kind PC, Isaac JTR, Daw MI. 2015. Experience-dependent, layer-specific development of divergent thalamocortical connectivity. *Cereb Cortex*. 25:2255–2266.

Del Rio-Bermudez C, Blumberg MS. 2018. Active sleep promotes functional connectivity in developing sensorimotor networks. *BioEssays*. 40:1700234.

Del Rio-Bermudez C, Kim J, Sokoloff G, Blumberg MS. 2017. Theta oscillations during active sleep synchronize the developing rubro-hippocampal sensorimotor network. *Curr Biol*. 27:1413–1424.

Del Rio-Bermudez C, Plumeau AM, Sattler NJ, Sokoloff G, Blumberg MS. 2016. Spontaneous activity and functional connectivity in the developing cerebellorubral system. *J Neurophysiol*. 116:1316–1327.

Del Rio-Bermudez C, Sokoloff G, Blumberg MS. 2015. Sensorimotor processing in the newborn rat red nucleus during active sleep. *J Neurosci*. 35:8322–8332.

Donato F, Jacobsen RI, Moser MB, Moser EI. 2017. Stellate cells drive maturation of the entorhinal-hippocampal circuit. *Science*. 355:eaai8178.

Dooley JC, Blumberg MS. 2018. Developmental “awakening” of primary motor cortex to the sensory consequences of movement. *elife*. 7:e41841.

Fox K. 1992. A critical period for experience-dependent synaptic plasticity in rat barrel cortex. *J Neurosci*. 12:1826–1838.

França ASC, do Nascimento GC, Lopes-dos-Santos V, Muratori L, Ribeiro S, Lobão-Soares B, Tort ABL. 2014. Beta2 oscillations (23–30 Hz) in the mouse hippocampus during novel object recognition. *Eur J Neurosci*. 40:3693–3703.

Fujisawa S, Buzsáki G. 2011. A 4 Hz oscillation adaptively synchronizes prefrontal, VTA, and hippocampal activities. *Neuron*. 72:153–165.

Gollo LL, Mirasso C, Sporns O, Breakspear M. 2014. Mechanisms of zero-lag synchronization in cortical motifs. *PLoS Comput Biol*. 10:e1003548.

Gretenkord S, Kostka JK, Hartung H, Watznauer K, Fleck D, Minier-Toribio A, Spehr M, Hanganu-Opatz IL. 2019. Coordinated electrical activity in the olfactory bulb gates the oscillatory entrainment of entorhinal networks in neonatal mice. *PLoS Biol*. 7:e2006994.

Grossberg S. 2009. Beta oscillations and hippocampal place cell learning during exploration of novel environments. *Hippocampus*. 19:881–885.

Hamada Y, Miyashita E, Tanaka H. 1999. Gamma-band oscillations in the "barrel cortex" precede rat's exploratory whisking. *Neuroscience*. 88:667–671.

Hanganu-Opatz IL. 2010. Between molecules and experience: role of early patterns of coordinated activity for the development of cortical maps and sensory abilities. *Brain Res Rev*. 64:160–176.

Hanganu IL, Staiger JF, Ben-Ari Y, Khazipov R. 2007. Cholinergic modulation of spindle bursts in the neonatal rat visual cortex in vivo. *J Neurosci*. 27:5694–5705.

Harrison MT, Geman S. 2009. A rate and history-preserving resampling algorithm for neural spike trains. *Neural Comput*. 21:1244–1258.

Hartung H, Brockmann MD, Pöschel B, De Feo V, Hanganu-Opatz IL. 2016a. Thalamic and entorhinal network activity differently modulates the functional development of prefrontal–hippocampal interactions. *J Neurosci*. 36:3676–3690.

Hartung H, Cichon N, De Feo V, Riemann S, Schildt S, Lindemann C, Mulert C, Gogos JA, Hanganu-Opatz IL. 2016b. From shortage to surge: a developmental switch in hippocampal-prefrontal coupling in a gene-environment model of neuropsychiatric disorders. *Cereb Cortex*. 26:4265–4281.

Igarashi KM, Lu L, Colgin LL, Moser MB, Moser EI. 2014. Coordination of entorhinal-hippocampal ensemble activity during associative learning. *Nature*. 510:143–147.

Inácio AR, Nasretdinov A, Lebedeva J, Khazipov R. 2016. Sensory feedback synchronizes motor and sensory neuronal networks in the neonatal rat spinal cord. *Nat Commun*. 7: 13060.

Itskov PM, Vinnik E, Diamond ME. 2011. Hippocampal representation of touch-guided behavior in rats: persistent and independent traces of stimulus and reward location. *PLoS One*. 6:e16462.

Khazipov R, Luhmann HJ. 2006. Early patterns of electrical activity in the developing cerebral cortex of humans and rodents. *Trends Neurosci*. 29:414–418.

Khazipov R, Sirota A, Leinekugel X, Holmes GL, Ben-Ari Y, Buzsaki G. 2004. Early motor activity drives spindle bursts in the developing somatosensory cortex. *Nature*. 432: 758–761.

Kilb W, Kirischuk S, Luhmann HJ. 2011. Electrical activity patterns and the functional maturation of the neocortex. *Eur J Neurosci*. 34:1677–1686.

Kilb W, Luhmann HJ. 2003. Carbachol-induced network oscillations in the intact cerebral cortex of the newborn rat. *Cereb Cortex*. 13:409–421.

Lahtinen H, Palva JM, Sumanen S, Voipio J, Kaila K, Taira T. 2002. Postnatal development of rat hippocampal gamma rhythm in vivo. *J Neurophysiol*. 88:1469–1474.

Lebedeva J, Zakharov A, Ogievetsky E, Minlebaeva A, Kurbanov R, Gerasimova E, Sitdikova G, Khazipov R. 2017. Inhibition of cortical activity and apoptosis caused by ethanol in neonatal rats in vivo. *Cereb Cortex*. 27:1068–1082.

Li W, Ma L, Yang G, Gan WB. 2017. REM sleep selectively prunes and maintains new synapses in development and learning. *Nat Neurosci*. 20:427–437.

Lipton SA, Kater SB. 1989. Neurotransmitter regulation of neuronal outgrowth, plasticity and survival. *Trends Neurosci*. 12:265–270.

Luhmann HJ, Khazipov R. 2018. Neuronal activity patterns in the developing barrel cortex. *Neuroscience*. 368:256–267.

Maggi L, Le Magueresse C, Changeux J-P, Cherubini E. 2003. Nicotine activates immature "silent" connections in the developing hippocampus. *Proc Natl Acad Sci*. 100:2059–2064.

Marrosu F, Portas C, Mascia MS, Casu MA, Fà M, Giagheddu M, Imperato A, Gessa GL. 1995. Microdialysis measurement of cortical and hippocampal acetylcholine release during sleep-wake cycle in freely moving cats. *Brain Res*. 671:329–332.

Martin C, Beshel J, Kay LM. 2007. An olfacto-hippocampal network is dynamically involved in odor-discrimination learning. *J Neurophysiol*. 98:2196–2205.

McVea DA, Mohajerani MH, Murphy TH. 2012. Voltage-sensitive dye imaging reveals dynamic spatiotemporal properties of cortical activity after spontaneous muscle twitches in the newborn rat. *J Neurosci*. 32:10982–10994.

Mohns EJ, Blumberg MS. 2008. Synchronous bursts of neuronal activity in the developing hippocampus: modulation by active sleep and association with emerging gamma and theta rhythms. *J Neurosci*. 28:10134–10144.

Mohns EJ, Blumberg MS. 2010. Neocortical activation of the hippocampus during sleep in infant rats. *J Neurosci*. 30:3438–3449.

Moser EI, Moser MB, McNaughton BL. 2017. Spatial representation in the hippocampal formation: a history. *Nat Neurosci*. 20:1448–1464.

Mukherjee D, Sokoloff G, Blumberg MS. 2018. Corollary discharge in precerebellar nuclei of sleeping infant rats. *elife*. 7:e38213.

Nebel MB, Joel SE, Muschelli J, Barber AD, Caffo BS, Pekar JJ, Mostofsky SH. 2012. Disruption of functional organization within the primary motor cortex in children with autism. *Hum Brain Mapp*. 35:567–580.

Pereira A, Ribeiro S, Wiest M, Moore LC, Pantoja J, Lin S-C, Nicolelis MAL. 2007. Processing of tactile information by the hippocampus. *Proc Natl Acad Sci*. 104:18286–18291.

Pugh PC, Margiotta JF. 2000. Nicotinic acetylcholine receptor agonists promote survival and reduce apoptosis of chick ciliary ganglion neurons. *Mol Cell Neurosci*. 15:113–122.

Rangel LM, Chiba AA, Quinn LK. 2015. Theta and beta oscillatory dynamics in the dentate gyrus reveal a shift in network processing state during cue encounters. *Front Syst Neurosci*. 9:96.

Seelke AMH, Blumberg MS. 2008. The microstructure of active and quiet sleep as cortical delta activity emerges in infant rats. *Sleep*. 31:691–699.

Seelke AMH, Dooley JC, Krubitzer LA. 2012. The emergence of somatotopic maps of the body in S1 in rats: the correspondence between functional and anatomical organization. *PLoS One*. 7:e32322.

Sei H, Saitoh D, Yamamoto K, Morita K, Morita Y. 2000. Differential effect of short-term REM sleep deprivation on NGF and BDNF protein levels in the rat brain. *Brain Res*. 877:387–390.

Simons DJ, Land PW. 1987. Early experience of tactile stimulation influences organization of somatic sensory cortex. *Nature*. 326:694–697.

Sokoloff G, Plumeau AM, Mukherjee D, Blumberg MS. 2015. Twitch-related and rhythmic activation of the developing cerebellar cortex. *J Neurophysiol*. 114:1746–1756.

Stam CJ, Nolte G, Daffertshofer A. 2007. Phase lag index: assessment of functional connectivity from multi channel EEG and MEG with diminished bias from common sources. *Hum Brain Mapp*. 28:1178–1193.

Teles-Grilo Ruivo LM, Baker KL, Conway MW, Kinsley PJ, Gilmour G, Phillips KG, Isaac JTR, Lowry JP, Mellor JR. 2017. Coordinated acetylcholine release in prefrontal cortex and hippocampus is associated with arousal and reward on distinct timescales. *Cell Rep*. 18:905–917.

Tiriac A, Blumberg MS. 2016. Gating of reafference in the external cuneate nucleus during self-generated movements in wake but not sleep. *elife*. 5:e18749.

Tiriac A, Del Rio-Bermudez C, Blumberg MS. 2014. Self-generated movements with "unexpected" sensory consequences. *Curr Biol*. 24:2136–2141.

Tiriac A, Uitermarkt BD, Fanning AS, Sokoloff G, Blumberg MS. 2012. Rapid whisker movements in sleeping newborn rats. *Curr Biol*. 22:2075–2080.

Uhlhaas P, Singer W. 2010. Developmental changes in neuronal oscillations and synchrony: evidence for a late critical period. In: Battro AM, Dehaene S, Singer WJ, editors. *Proceedings of the Working Group on Human Neuroplasticity and Education*. Vatican City: The Pontifical Academy of Sciences, pp. 218–229.

Uhlhaas PJ, Roux F, Rodriguez E, Rotarska-Jagiela A, Singer W. 2010. Neural synchrony and the development of cortical networks. *Trends Cogn Sci*. 14:72–80.

Valeeva G, Janackova S, Nasretdinov A, Rychkova V, Makarov R, Holmes GL, Khazipov R, Lenck-Santini P-P. 2018. Emergence of coordinated activity in the developing entorhinal-hippocampal network. *Cereb Cortex*. 3:1–15.

Vicente R, Gollo LL, Mirasso CR, Fischer I, Pipa G. 2008. Dynamical relaying can yield zero time lag neuronal synchrony despite long conduction delays. *Proc Natl Acad Sci*. 105:17157–17162.

Vinck M, Bos JJ, Van Mourik-Donga LA, Oplaat KT, Klein GA, Jackson JC, Gentet LJ, Pennartz CMA. 2016. Cell-type and state-dependent synchronization among rodent somatosensory, visual, perirhinal cortex, and hippocampus CA1. *Front Syst Neurosci*. 9:187.

Vinogradova OS. 2001. Hippocampus as comparator: role of the two input and two output systems of the hippocampus in selection and registration of information. *Hippocampus*. 11:578–598.

Whyatt C, Craig C. 2013. Sensory-motor problems in autism. *Front Integr Neurosci*. 7:1–12.

Wikstrom S, Iyer KK, Roberts JA, Hellstro L, Pupp IH, Ley D, Vanhatalo S, Breakspear M. 2015. Cortical burst dynamics predict clinical outcome early in extremely preterm infants. *Brain*. 138:2206–2218.

Yang JW, Reyes-Puerta V, Kilb W, Luhmann HJ. 2016. Spindle bursts in neonatal rat cerebral cortex. *Neural Plast*. 2016:3467832.

SUPPLEMENTARY FIGURES

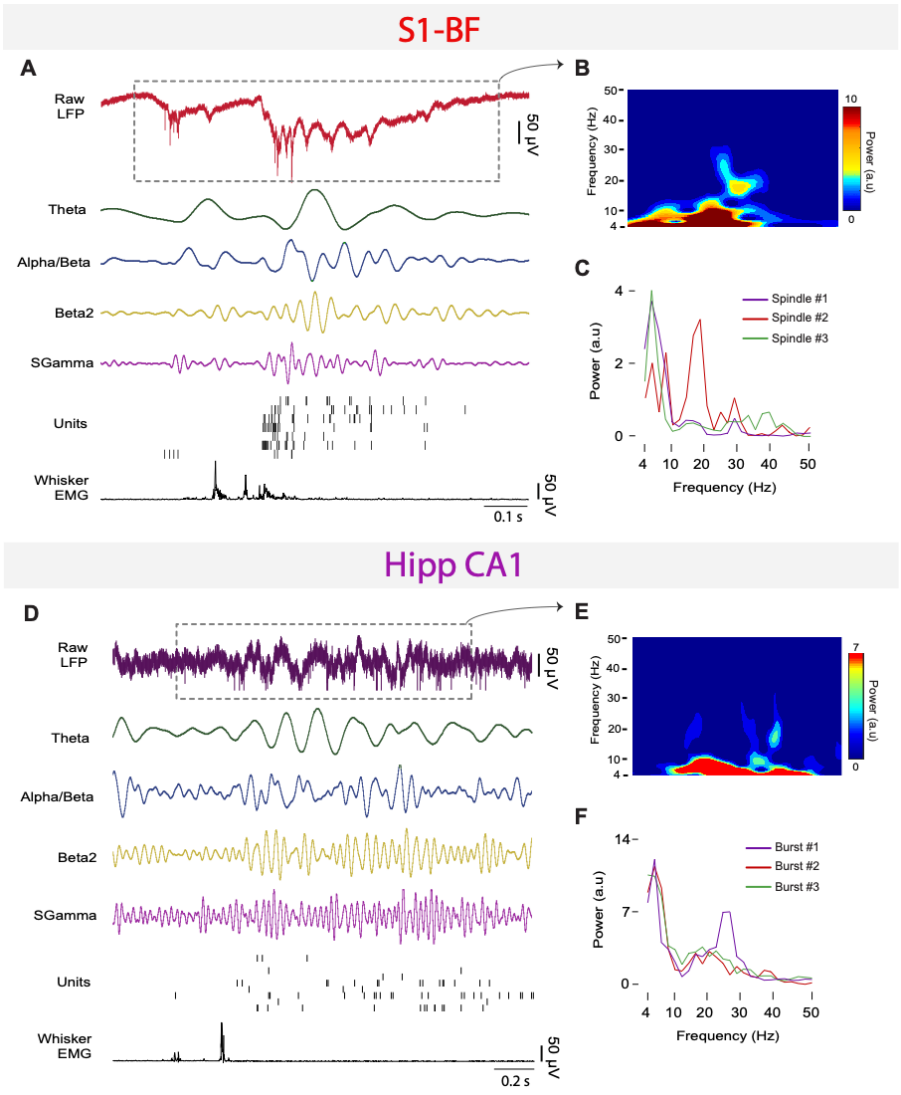

Figure S1. Oscillatory bursts in S1-BF and Hipp CA1 are composed of multiple frequency bands. (A) Representative spindle burst during AS recorded from S1-BF in a P8 rat. Depicted is the raw LFP (red trace) and corresponding filtered signals (theta, alpha/beta, beta2, and sgamma), unit activity (black tick marks), and whisker EMG (black trace) in response to a whisker twitch. (B) Time-frequency spectrogram for the raw LFP signal in (A) denoted by the dashed rectangle. (C) Power spectra corresponding to three representative spindle bursts recorded from S1-BF. (D) Representative oscillatory burst in Hipp CA1 during AS in a P8 rat. All the signals depicted here are the same as those in (A). (E) Time-frequency spectrogram for the raw LFP signal in (D) denoted by the dashed rectangle. (F) Power spectra corresponding to three representative bursts recorded from Hipp CA1.

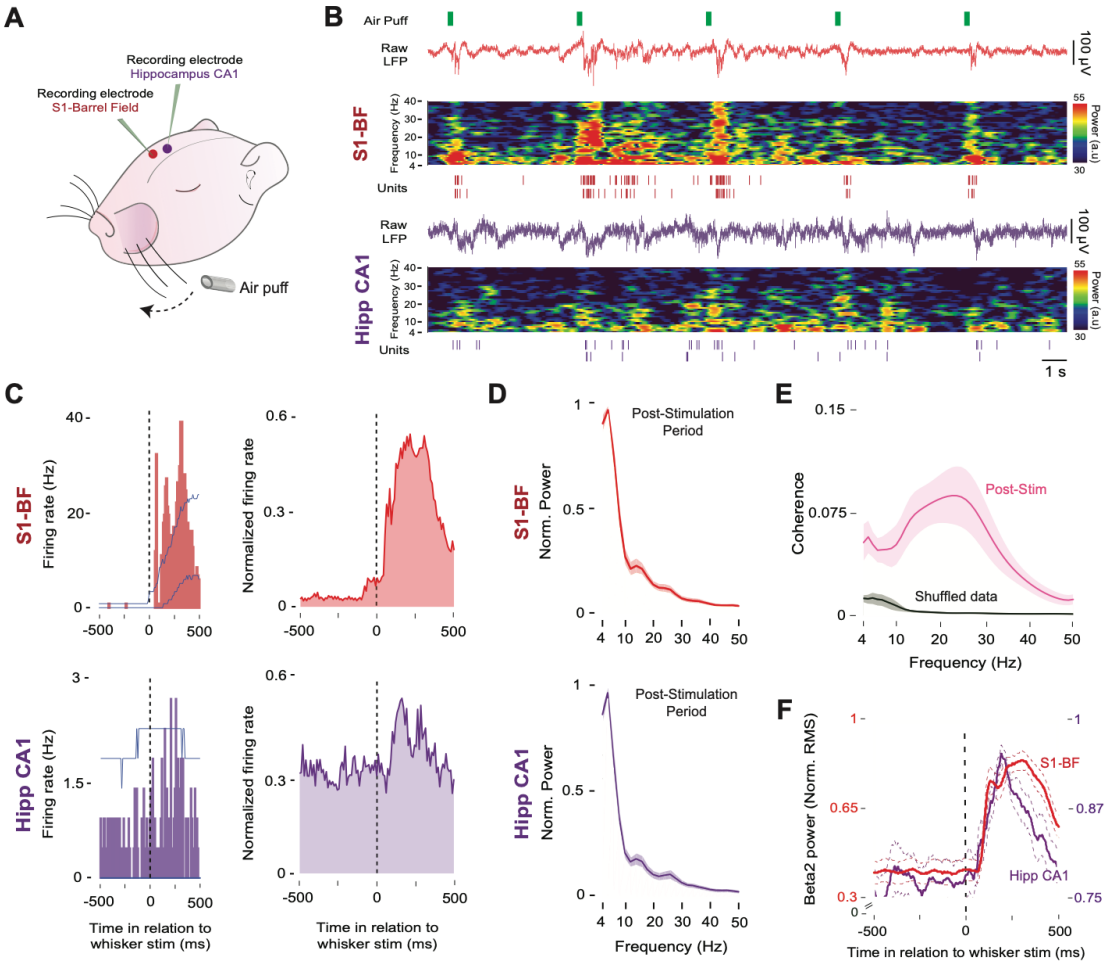

Figure S2. Exafferent stimulation of the whiskers triggers neural responses in S1-BF and Hipp CA1 at P8. (A) Illustration depicting whisker stimulation using air puffs and simultaneous recordings of S1-BF and Hipp CA1 in a P8 rat. (B) Representative data depicting raw LFP activity, corresponding time-frequency spectrogram, and unit activity in response to whisker stimulation in S1-BF (top, red traces) and Hipp CA1 (bottom, purple traces) in a P8 rat. Green tick marks denote stimulus onset. (C) Representative perievent histograms (10-ms bins) for spike activity in relation to whisker stimulation in S1-BF (red, top) and Hipp CA1 (purple, bottom) in a P8 rat. Vertical dashed lines indicate stimulus onset. Upper and lower acceptance bands ($p < 0.05$) are indicated by blue lines. Right: Same as in (left) for normalized pooled data across all units that exhibited significant stimulus-related activity ($p < 0.05$) in S1-BF (n = 84 units) and Hipp CA1 (n = 13 units). (D) Mean normalized power spectra for LFP activity following whisker stimulation (500-ms window) for S1-BF (top) and Hipp CA1 (bottom). Shaded area indicates SE. Vertical line in spectrograms denotes whisker twitch onset. (E) Mean LFP-LFP coherence spectra between S1-BF and Hipp CA1 following whisker stimulation (pink) and for shuffled data (black) Shaded area indicates SE. (F) Mean normalized stimulation-triggered LFP power (beta2; 20-30 Hz; root mean square) pooled across subjects for S1-BF (red) and Hipp CA1 (purple). Dotted lines indicate SE.

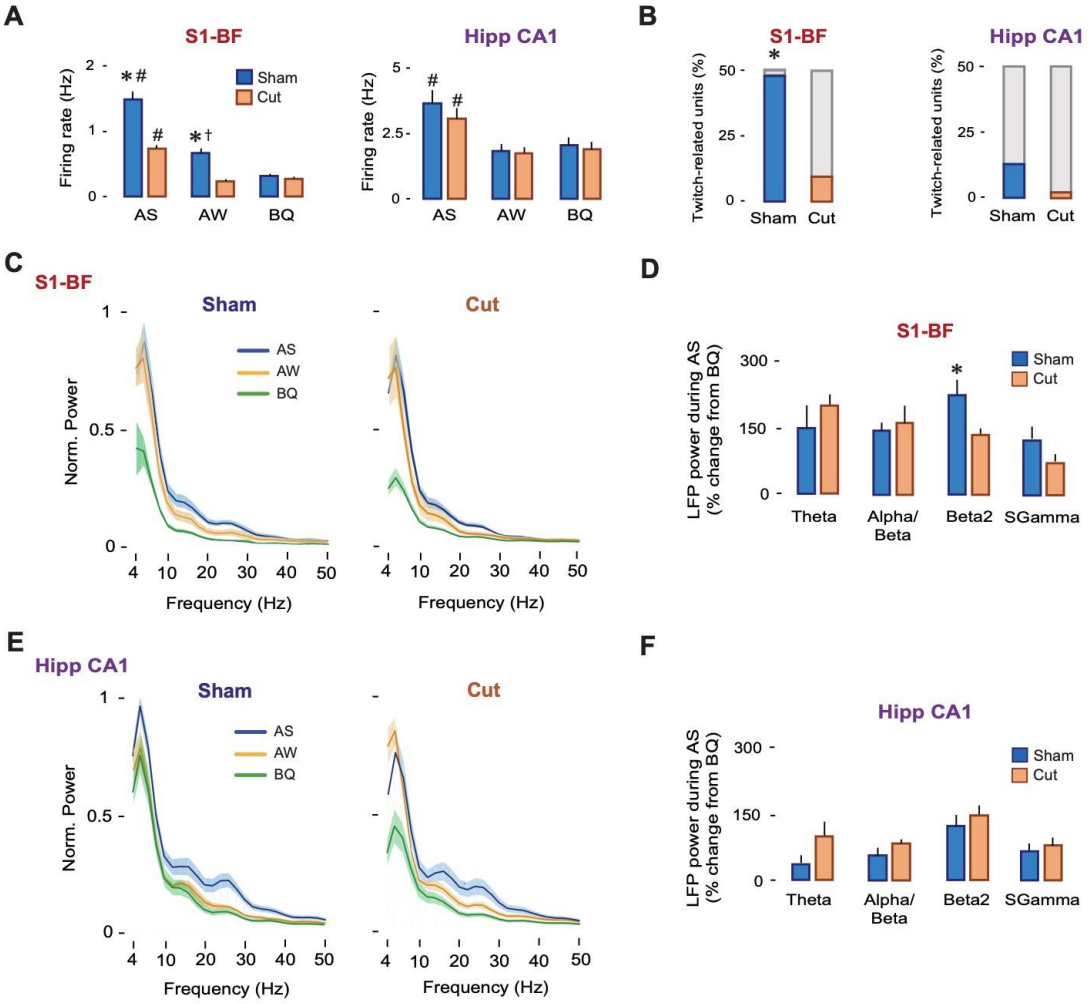

Figure S3. Effects of ION transection on spontaneous neural activity in S1-BF and Hipp CA1. (A) Mean (+SE) firing rates in S1-BF (top) and Hipp CA1 (bottom) in the Sham (blue) and Cut (orange) groups across behavioral states (AS, AW, BQ). * significant difference from Cut group within a behavioral state ($p < 0.001$). # significant difference from AW and BQ within the same experimental group ($p < 0.001$). † significant difference from BQ within the same experimental group ($p < 0.001$). (B) Stacked plots indicating percentage of all units in S1-BF (top) and Hipp CA1 (bottom) that were significantly twitch-related in the Sham (blue) and Cut (orange) groups. The percentage of twitch-related units in S1-BF was significantly lower (χ^2 (1, N = 107) = 19.8, $p < 0.0001$) in the Cut group (9.5%, 6/63 units) than in the Sham group (47.7%, 21/44 units). In Hipp CA1, 2.2% of units (1/46) were responsive to whisker twitches in the Cut group, as compared with 12.9% of units (4/31) in the Sham group (χ^2 (1, N = 77) = 3.4, $p = 0.06$. * significant difference from Cut group, $p < 0.0001$. (C) Mean power spectra of LFP activity in S1-BF during AS (blue), AW (orange), and BQ (green) in the Sham (left) and Cut (right) groups. Shaded area represents SE. (D) Mean (+ SE) percent change in LFP power in S1-BF during AS in relation to BQ across frequency bands in the Sham (blue) and Cut (orange) groups. * significant difference from Cut group, $p < 0.05$. (H) Same as in (G) but for Hipp CA1 activity. (E) Same as in (C) but for LFP activity in Hipp CA1. (F) Same as in (D) but for LFP power in Hipp CA1.